High-throughput sequencing reveals a simple model of nucleosome energetics

George Locke[a], Denis Tolkunov[a], Zarmik Moqtaderi[b], Kevin Struhl[b], and Alexandre V. Morozov[a,1]

[a]Department of Physics and Astronomy and BioMaPS Institute for Quantitative Biology, Rutgers University, Piscataway, NJ 08854; and [b]Department of Biological Chemistry and Molecular Pharmacology, Harvard Medical School, Boston, MA 02115

Edited* by Eric Dean Siggia, The Rockefeller University, New York, NY, and approved September 13, 2010 (received for review March 22, 2010)

We use genome-wide nucleosome maps to study sequence specificity of intrinsic histone-DNA interactions. In contrast with previous approaches, we employ an analogy between a classical one-dimensional fluid of finite-size particles in an arbitrary external potential and arrays of DNA-bound histone octamers. We derive an analytical solution to infer free energies of nucleosome formation directly from nucleosome occupancies measured in high-throughput experiments. The sequence-specific part of free energies is then captured by fitting them to a sum of energies assigned to individual nucleotide motifs. We have developed hierarchical models of increasing complexity and spatial resolution, establishing that nucleosome occupancies can be explained by systematic differences in mono- and dinucleotide content between nucleosomal and linker DNA sequences, with periodic dinucleotide distributions and longer sequence motifs playing a minor role. Furthermore, similar sequence signatures are exhibited by control experiments in which nucleosome-free genomic DNA is either sonicated or digested with micrococcal nuclease, making it possible that current predictions based on high-throughput nucleosome-positioning maps are biased by experimental artifacts.

chromatin structure | histone-DNA interactions | nucleosome positioning | biophysical models

In eukaryotes, 75%–90% of genomic DNA is packaged into histone-DNA complexes called nucleosomes, with adjacent nucleosomes separated by stretches of linker DNA (1). Each nucleosome consists of 147 base pairs (bp) of DNA wrapped around a histone octamer in a left-handed superhelix (2). Arrays of nucleosomes fold into filamentous chromatin fibers which constitute building blocks for higher-order structures (3). DNA wrapped in a nucleosome is occluded from interacting with other DNA-binding proteins such as transcription factors, RNA polymerase, and DNA repair complexes (2). On the other hand, histone tail domains act as substrates for posttranslational modifications, providing binding sites for chromatin-associated proteins which facilitate transitions between active and silent chromatin states (4).

Several distinct factors affect nucleosome positions in living cells. First of all, intrinsic histone-DNA interactions are sequence-specific: for example, poly(dA:dT) tracts are well known to disfavor nucleosome formation (5, 6). In addition, nucleosome-depleted regions can be generated through the action of ATP-dependent chromatin remodeling enzymes (7) and histone acetylases (8). Finally, non-histone DNA-binding factors can alter nucleosome positions through binding their cognate sites and either displacing nucleosomes or hindering their subsequent formation (9, 10).

The nucleosome code hypothesis states that DNA sequence is the primary determinant of nucleosome positions in living cells (11). This hypothesis is often contrasted with the idea of statistical positioning which asserts that most nucleosomes are ordered into regular arrays simply by steric exclusion (12, 13). In this view the nucleosomal arrays are "phased" by external boundaries such as DNA-bound factors or DNA sequences unfavorable for nucleosome formation. It is also possible that a small number of nucleosomes with favorable binding affinities create boundaries against which neighboring nucleosomes are ordered by steric exclusion (14, 15).

Nucleosome positioning can be thought of as rotational, referring to the 10–11 bp-periodic orientation of the DNA helix with respect to the surface of the histone octamer, and translational, referring to the 147 bp-long sequence covered by a particular histone octamer. Optimal rotational positioning minimizes free energy of anisotropic DNA bending, causing 10–11 bp periodicity of dinucleotide frequencies in nucleosome-positioning sequences (16). We use a probabilistic description of translational positioning in which 147 bp sites with favorable free energies of nucleosome formation have a higher probability to form nucleosomes.

To study the contribution of intrinsic histone-DNA interactions to nucleosome positioning, several computational models based solely on the DNA sequence have been proposed. These models can be divided into bioinformatics, which are trained on sets of nucleosomal sequences obtained from living cells (11, 17–21) or from in vitro reconstitution experiments (5), and ab initio, which predict nucleosome energies and occupancies using DNA elasticity theory and structural data (22–24).

Here we develop a physical model for predicting free energies of nucleosome formation directly from high-throughput maps of nucleosome positions. Unlike previous approaches, our model employs an exact relation between measured nucleosome occupancies and free energies, treating steric exclusion rigorously in the presence of histone-DNA interactions of arbitrary strength and sequence specificity. We focus in particular on nucleosomes reconstituted in vitro on yeast genomic DNA (5, 25). In this case nucleosome locations are affected solely by intrinsic histone-DNA interactions and by formation of higher-order chromatin structures. To determine whether current nucleosome-positioning maps are biased by experimental artefacts, we compare our predictions with sequence signals from two nucleosome-free control experiments in which DNA was either sonicated or digested with micrococcal nuclease (MNase) to yield mononucleosome-size segments. We also test the ability of our in vitro model to predict nucleosome positions in vivo, and study the universality of nucleosome-positioning motifs by applying our approach to other organisms.

Results

Biophysical Model of Nucleosome Occupancy and Energetics. We have predicted histone-DNA interaction energies genome-wide using an analogy between arrays of nucleosomes and a one-dimensional

Author contributions: G.L., K.S., and A.V.M. designed research; G.L. and D.T. performed research; Z.M. contributed new reagents/analytic tools; G.L., D.T., Z.M., and A.V.M. analyzed data; and G.L. and A.V.M. wrote the paper.

The authors declare no conflict of interest.

*This Direct Submission article had a prearranged editor.

Data deposition: The data reported in this paper have been deposited in the Gene Expression Omnibus (GEO) database, www.ncbi.nlm.nih.gov/geo.

[1]To whom correspondence should be addressed. E-mail: morozov@physics.rutgers.edu.

This article contains supporting information online at www.pnas.org/lookup/suppl/doi:10.1073/pnas.1003838107/-/DCSupplemental.

fluid of nonoverlapping particles of size 147 bp in an arbitrary external potential. For such a fluid it was shown by Jerry K. Percus that particle energies can be inferred exactly from the density profile (26). Although our method neglects formation of three-dimensional chromatin structures which may cause linker DNA to adopt preferred lengths (27, 28), it rigorously takes into account both steric exclusion between neighboring particles and intrinsic histone-DNA interactions, including the 10–11 bp-periodic rotational component. Our approach, outlined in Fig. S1, proceeds in the direction opposite to previous work which first employed either bioinformatics or DNA elastic theory to construct a sequence-specific histone-DNA interaction potential and then positioned nucleosomes on genomic DNA without steric overlap (5, 11, 18, 22). In contrast, we employ an exact decomposition from experimentally available nucleosome probabilities and occupancies to free energies of nucleosome formation which we call Percus energies (Eq. **1**).

To extract the sequence-specific component of nucleosome energetics, we fit Percus energies at each genomic bp to a sum of energies of individual nucleotide motifs ranging from 1 to N bp in length (see *Materials and Methods*). There is no need to construct an explicit background model of word frequencies with this approach, and the linear fit is guaranteed to converge to the globally optimal solution. Thus Percus decomposition allows us to bypass a nonlinear fit of motif energies to the occupancy profile. Words with the same nucleotide sequence are assumed to have the same energy if they occur anywhere in the 147 bp-long nucleosomal site (the position-independent model, Eq. **2**), or fall into one of the three equal-length regions that span the 147 bp site (the three-region model), or are separated by an integer multiple of the 10 bp DNA helical twist (the periodic model). All models are constrained to assign nonzero energies to words with N nucleotides only if the sequence specificity of Percus energies cannot be captured using words with $1 \ldots N-1$ nucleotides (see *SI Text*). We refer to the maximum length of the words included into a model as its *order* N. In addition, we have developed an order 2 model in which mono- and dinucleotides are allowed to have different energies at every position in the 147 bp-long nucleosomal site (the spatially resolved model, Eq. **3**).

We have used the sequence-specific models to predict nucleosome formation energies for *Saccharomyce cerevisiae*, *Caenorhabditis elegans*, and *Escherichia coli*. These energies serve as input to a recursive algorithm which computes the probability to start a nucleosome and the nucleosome occupancy (defined as the probability that a given bp is covered by any nucleosome) at every genomic bp (11, 22).

A:T/G:C Content Is the Primary Determinant of Nucleosome Sequence Preferences in *S. cerevisiae*. The $N = 5$ position-independent model, which assigns energies to 364 independent words ranging from 1 bp to 5 bp in length, is capable of accurately predicting occupancy by nucleosomes assembled in vitro on yeast genomic DNA (Fig. S2 *A* and *B*). Remarkably, even though the model is based on Zhang et al. high-throughput nucleosome-positioning data (25) (yielding $r = 0.61$ between predicted and observed occupancies), its prediction of Kaplan et al. in vitro occupancies (5) is more accurate ($r = 0.75$), partially due to the 2.85-fold higher sequence coverage in the latter dataset. Indeed, the correlation coefficient drops from 0.75 to 0.70 when sequence reads are randomly removed from the Kaplan et al. map to match Zhang et al. level of read coverage. These correlations are highly significant: randomizing sequence read positions and creating random nucleosome arrays typically yields $r < 0.1$ with measured occupancies. The correlation between the two in vitro datasets themselves is rather low ($r = 0.69$), probably because Kaplan et al. used 0.4:1 histone-to-DNA mass ratio, whereas Zhang et al. employed 1:1 ratio which corresponds to in vivo levels of nucleosome occupancy (5, 25).

The $N = 5$ model is also highly successful in discriminating between high- and low-occupancy regions (dashed curves in Fig. 1*B*). Its performance is comparable to the Kaplan et al. bioinformatics model (5) which takes both distributions of 5 bp-long words in nucleosomes and linkers and position-dependent dinucleotide frequencies into account (Table S1 and Dataset S1, dashed-dotted curves in Fig. 1*B*). Occupancies predicted by the two models are highly correlated ($r = 0.89$) and thus capture essentially the same nucleosome sequence preferences. Note that we report correlations between occupancy profiles while Kaplan et al. perform a log-transform on occupancies before computing a linear correlation coefficient: as a result we obtain $r = 0.79$ between Kaplan et al. predicted and in vitro occupancies, whereas they report $r = 0.89$ for the same comparison (5).

However, we find that using 5 bp-long words is not necessary: $N = 2$ position-independent model is virtually identical to the $N = 5$ model in predicting in vitro nucleosome occupancies (Fig. 1 *A* and Fig. S2*C*), classifying high- and low-occupancy re-

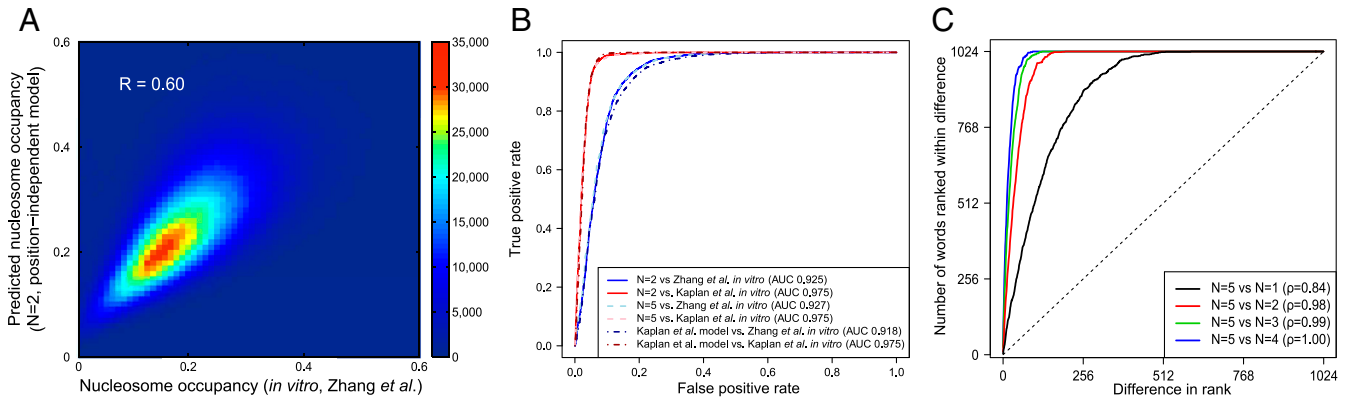

Fig. 1 Position-independent model predicts in vitro nucleosome occupancy in *S. cerevisiae* with high accuracy. (*A*) Density scatter plot for the nucleosome occupancy at each genomic base pair predicted with the $N = 2$ position-independent model vs. in vitro occupancy observed by Zhang et al. (25). The color of each region represents the number of data points mapped to that region. The model is fit on this data (see *Materials and Methods*). (*B*) The receiver operating characteristic curve for discriminating between DNA segments with high and low nucleosome occupancy. The yeast genome was parsed into 500 bp windows and the average nucleosome occupancy was computed for each window. 5,000 windows with the highest and 5,000 with the lowest average occupancies were ranked high-to-low using occupancies predicted with the $N = 2$ position-independent model, $N = 5$ position-independent model, and Kaplan et al. model (5). For each partial list of ranked windows with 1,…,10,000 entries we plot the fraction of windows in the list known to have high occupancy on the y-axis, low occupancy on the x-axis. (*C*) Rank-order plots of energies of 5 bp words: the energy of each word is ranked using position-independent models of order $N = 1$ through $N = 4$ and compared with the $N = 5$ model. Each curve shows the number of words whose ranks are separated by a given distance or less. ρ is the Spearman rank correlation coefficient.

gions (solid curves in Fig. 1*B*), and ranking 5 bp-long sequences (Fig. 1*C*). The $N = 2$ model remains highly correlated with the Kaplan et al. bioinformatics model ($r = 0.89$; Fig. S3). Remarkably, even the $N = 1$ position-independent model with one free parameter ($\epsilon_A = \epsilon_T$ and $\epsilon_C = \epsilon_G$ if both DNA strands are included for each mapped nucleosome) retains most of the predictive power of the higher-order models (Fig. 1*C* and Table S1), in agreement with two recent studies (20, 29). Thus positions of nucleosomes reconstituted in vitro on the yeast genome are largely controlled by the differences in A:T and G:C dinucleotide frequencies in nucleosomes and linkers. In particular, higher-order terms play little role in the energetics of poly(dA:dT) tracts (Fig. S4).

Indeed, Fig. 2 *A* and *B* show that DNA sequences of well-positioned nucleosomes (defined by five or more sequence reads mapped to the same genomic coordinate) are characterized by sharp A:T/G:C discontinuities across the nucleosome boundary. Overall, A:T dinucleotides are depleted in nucleosomes and enriched in linkers, with the opposite trend for G:C dinucleotides. Although well-positioned nucleosomes make up only 5.4% of all mapped nucleosomes defined by one or more sequence reads, they produce an occupancy profile which is highly correlated with the total nucleosome occupancy ($r = 0.71$, with 56.4% of genomic bps covered by at least one well-positioned nucleosome). In contrast, 81.5% of all nucleosomes are defined by just one or two reads and exhibit little sequence specificity (dashed lines in Fig. 2*A*). Furthermore, the $N = 2$ position-independent model based only on well-positioned nucleosomes is virtually identical to the $N = 2$ model based on all nucleosomes (rank correlation of 0.95 between the two sets of dinucleotide energies). Occupancies predicted by the two models correlate with $r = 0.997$. Thus our predictions reveal sequence preferences of a subset of nucleosomes that tend to occupy specific sites on the DNA.

Periodic Motif Distributions Do Not Play a Significant Role in Nucleosome Occupancy Predictions. Besides the A:T/G:C discontinuities, Fig. 2 *A* and *B* reveal two additional features that could affect positioning preferences of yeast nucleosomes: prominent 10–11 bp dinucleotide periodicity and a particularly strong A:T depletion and G:C enrichment within 20 bp of the nucleosome dyad. To test the utility of these features in nucleosome occupancy predictions we have employed three additional models that either partially or fully differentiate between words located at different positions within the nucleosomal site.

The three-region model assigns different energies to words found in the 47 bp-long core and flanking regions and is thus capable of capturing prominent dinucleotide biases in the vicinity of the nucleosomal dyad. The periodic model enforces 10 bp helical twist periodicity. The most detailed spatially resolved model captures all three main features exhibited by the frequencies of dinucleotides found in nucleosome-positioning sequences (Fig. 2*C*). These models do not offer a significant improvement over the $N = 2$ position-independent model (Table S1 and Dataset S1), reflecting the fact that all three features are simultaneously present in well-positioned in vitro nucleosomes (Fig. 2*A*) and so basing a prediction on any one of them is sufficient. Furthermore, global A:T/G:C discontinuities appear to play a role of the primary nucleosome-positioning determinant, whereas periodic oscillations of dinucleotide frequencies can be greatly diminished or absent in other organisms and in in vivo nucleosome-positioning maps from yeast (Fig. S5).

However, the rotational positioning component of the yeast model should be more predictive for nucleosomes positioned on DNA sequences with prominent 10–11 bp dinucleotide periodicities. Indeed, the spatially resolved model works better than the $N = 2$ position-independent model for six nucleosomes whose in vitro positions on short (<250 bp) DNA sequences have been determined with single bp precision by hydroxyl radical footprinting (Fig. S6). However, the predictive power is still modest, indicating that our approach is better suited to predicting nucleosome occupancies rather than exact positions of individual core particles.

In Vivo Nucleosome Positions Are Partially Controlled by the Underlying DNA Sequence. We investigated whether the simple rules that govern in vitro nucleosome positions remain valid in living cells. Indeed, in vivo nucleosomes appear to be well positioned in the vicinity of transcription start and termination sites, with prominent nucleosome-depleted regions (NDRs) on both ends of the transcript (Fig. S7; in vivo chromatin comes from cells grown in YPD medium) (5). In contrast, in vitro nucleosomes are much more delocalized (Fig. S8), so that nucleosomal arrays around NDRs are not ordered and NDRs themselves are much less pronounced (Fig. S7) (25).

Despite these differences, dinucleotide energies extracted from in vitro and in vivo nucleosome-positioning maps are reasonably well correlated (Fig. S9), yielding nearly identical predictions of nucleosome occupancies (Table S1). Although dinucleotide energies inferred from the in vivo map of cross-linked nucleosomes are not as close to their in vitro counterparts as the

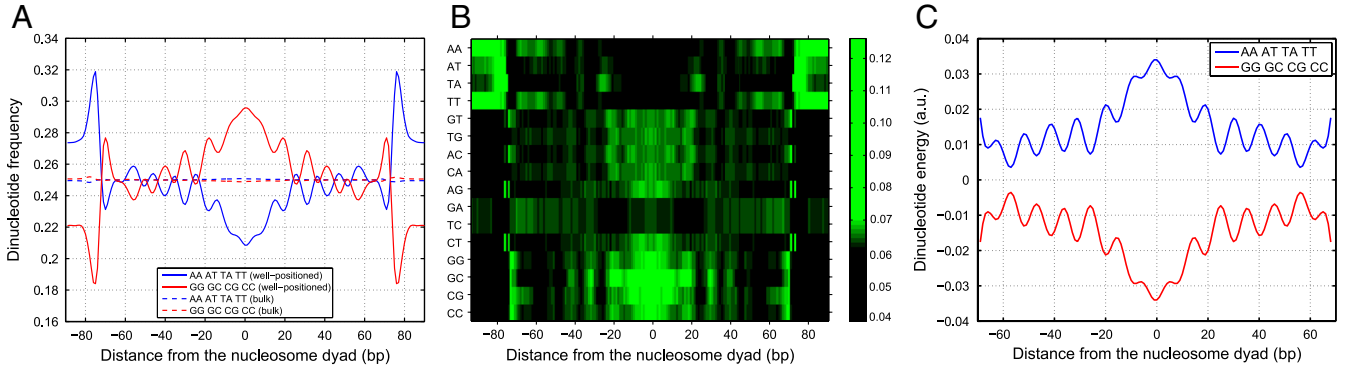

Fig. 2. Dinucleotide distributions in nucleosome and linker sequences. Nucleosomes were assembled in vitro on the yeast genome using salt dialysis (25). (*A*) Average relative frequencies of WW (AA, TT, AT, and TA) and SS (CC, GG, CG, and GC) dinucleotides at each position within the nucleosome are plotted with respect to the nucleosome dyad. The relative frequency of each dinucleotide is defined as its frequency at a given position divided by genome-wide frequency. All frequencies are smoothed using a 3 bp moving average. Solid lines: well-positioned nucleosomes defined by five or more sequence reads, dashed lines: bulk nucleosomes defined by one or two sequence reads. (*B*) Heat map of relative frequencies for each dinucleotide, plotted with respect to the nucleosome dyad. (*C*) Average energies of WW (AA, TT, AT, and TA) and SS (CC, GG, CG, and GC) dinucleotides at each position within the nucleosome predicted with the $N = 2$ spatially resolved model are plotted with respect to the nucleosome dyad.

energies based on the in vivo map without cross-linking, the two in vivo models yield very similar occupancy profiles ($r = 0.94$). We conclude that intrinsic sequence preferences cannot create the striking oscillations observed in the in vivo occupancy profile (Fig. S7). Rather, biological factors such as components of transcription initiation machinery may act to position the first nucleosome downstream of the NDR [the so-called +1 nucleosome (14)] (25).

Energetics of Nucleosome Formation in *E. coli* and *C. elegans*. To study whether dinucleotide-based nucleosome-positioning patterns observed in *S. cerevisiae* extend to other organisms, we have inferred position-independent dinucleotide energies from a map of nucleosomes assembled in vitro on the *E. coli* genome (25). Although the correlation between observed and predicted occupancies was modest in this case (Fig. 3*B*), probably because the *E. coli* genome did not evolve to favor nucleosome formation (resulting in lower sequence read coverage in competition with yeast DNA), the dinucleotide energies were similar in yeast and *E. coli* (Fig. 3*C*). The most prominent difference was exhibited by the four C:G-containing dinucleotides which have the lowest energies in *S. cerevisiae* but occupy middle positions in the case of *E. coli* (Table S2).

Dinucleotide energies inferred from the in vivo map of *C. elegans* nucleosomes (30), while an excellent predictor of nucleosome occupancies in the *C. elegans* genome (Fig. 3*A*), are even further from their yeast counterparts, with C:G-containing dinucleotides again affected most (Fig. 3*C* and Table S2). It is likely that in vivo effects override intrinsic nucleosome preferences in *C. elegans*. In addition, we find that the mononucleotide model is much less predictive in this organism: compared with the $N = 2$ position-independent model, the correlation between the $N = 1$ model and data is 30.8% worse in *C. elegans* but only 10.0% worse in yeast. On the other hand, fitting energies of 3 bp-long words in *C. elegans* resulted only in a 3.0% improvement in the correlation coefficient, indicating that it is not necessary to keep track of higher-order motifs.

Although the dinucleotide energies are somewhat different in the three organisms we examined, position-independent models from one organism can still be used to predict nucleosome positions in another. For example, using the $N = 2$ *E. coli* model to predict in vitro nucleosome occupancies in *S. cerevisiae* (25) results in $r = 0.55$, which is only a little worse than $r = 0.60$ observed with the "native" model (Table S1). The $N = 2$ *C. elegans* model has a correlation of 0.46 with the in vitro occupancy from *S. cerevisiae*, while the correlation between the $N = 2$ *S. cerevisiae* in vitro model and the in vivo occupancy from *C. elegans* is 0.52, somewhat lower than 0.65 obtained with the native model. Therefore it is possible to make useful predictions in organisms for which high-throughput nucleosome-positioning maps are not yet available.

Nucleosome-Free Control Experiments Can Be Used to Predict Nucleosome Positions. Depletion of A:T and enrichment of G:C-containing dinucleotides in nucleosomal sequences and the discontinuity of dinucleotide frequencies across the nucleosome boundary may be exaggerated by MNase sequence specificity —MNase is well known to preferentially digest A:T-rich sequences through its exonuclease activity (31, 32). To study this possibility, we have partially digested naked DNA from *S. cerevisiae* and *E. coli* genomes with MNase, isolated ~150 bp DNA fragments, and sequenced them. We have also examined another control in which DNA was sonicated rather than MNase-digested (25). We have computed Percus energies for these control experiments and analyzed their sequence specificity using the $N = 2$ position-independent model.

Unexpectedly, in both cases predicted dinucleotide energies are very close to those obtained from in vitro nucleosome-positioning maps (Fig. 4*A*). The differences are comparable to those between the $N = 2$ in vitro and in vivo models (Fig. S9). As a result, the $N = 2$ model trained on yeast sequences from the sonication and MNase controls predicts Kaplan et al. in vitro nucleosome occupancies with correlation coefficients of 0.64 and 0.61, respectively, compared with $r = 0.75$ for the model trained on Zhang et al. in vitro nucleosomes (Table S1). The $N = 2$ model trained on *E. coli* sequences from the sonication and MNase controls yields 0.67 and 0.42 (Dataset S1).

One explanation for the predictive power of the MNase control is that dinucleotide energies assigned to nucleosomes are biased to some extent by sequence specificity of MNase exonuclease activity. Alternatively, exonuclease activity of MNase may simply isolate nucleosomal sequences fortuitously, without causing substantial loss of nucleosomes occupying A:T-rich DNA. The distribution of dinucleotides frequencies in MNase-digested DNA of mononucleosome size is somewhat similar to that observed in nucleosomes, although there are also substantial differences (cf. Fig. 2*A* and Fig. 4*B*). In particular, MNase-digested sequences given by more than five sequence reads coincide with well-positioned in vitro nucleosomes from Zhang et al. (defined by five or more sequence reads) 3.5 times more frequently than expected by chance. We also find that sonicated sequences are A:T-depleted and G:C-enriched, although in contrast with MNase the deviations of dinucleotide frequencies from their genome-wide averages are rather small (Fig. S5*F*). Apparently, sonication tends to break DNA segments across the A:T/G:C "fault lines" which also define nucleosome boundaries,

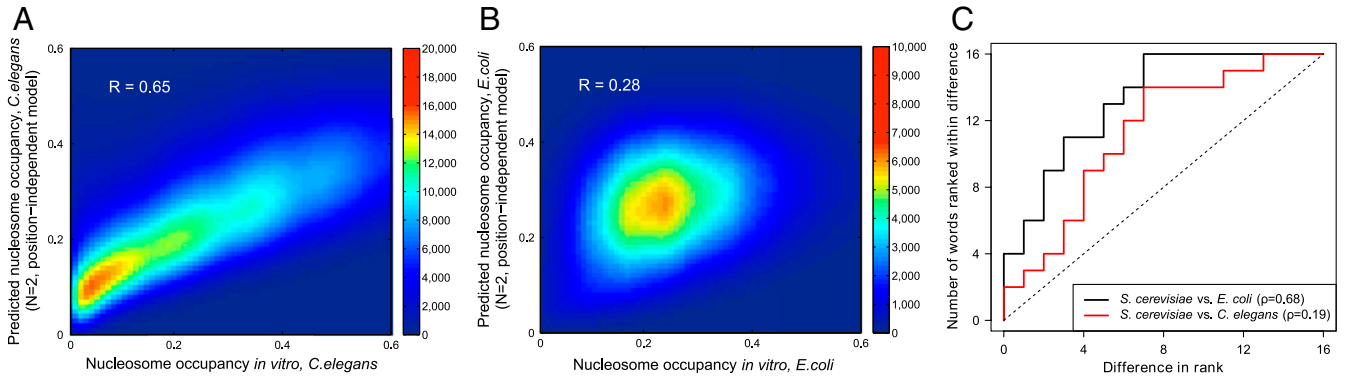

Fig. 3. Prediction of nucleosome occupancies in *C. elegans* and *E. coli*. Density scatter plots for the nucleosome occupancy at each genomic base pair predicted with the $N = 2$ position-independent model vs. in vivo occupancy in *C. elegans* (30) (*A*) and in vitro occupancy in *E. coli* (25) (*B*). Rank-order plots of energies of 2 bp words (*C*): the energy of each word is ranked using a position-independent model of order $N = 2$ trained on either in vitro (*S. cerevisiae*, *E. coli*) or in vivo (*C. elegans*) nucleosome-positioning data. Each curve shows the number of words whose ranks are separated by a given distance or less in the *C. elegans* and *E. coli* vs. *S. cerevisiae* fits. ρ is the Spearman rank correlation coefficient.

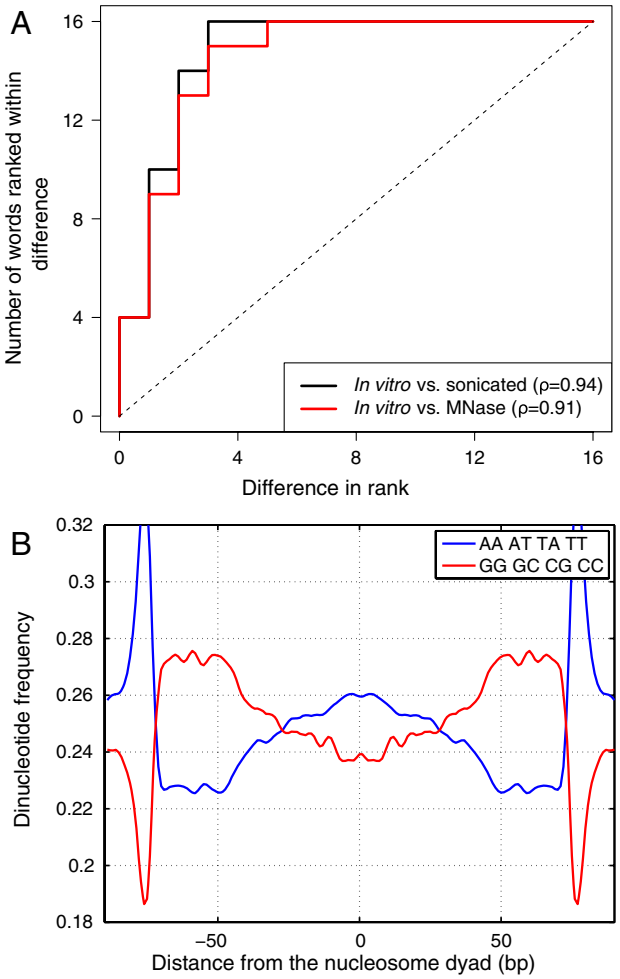

Fig. 4. Nucleosome-free control experiments yield sequences with nucleosome-like dinucleotide distributions. (*A*) Rank-order plots of energies of 2 bp words: the energy of each word is ranked using a position-independent model of order $N = 2$ trained on either in vitro nucleosome-positioning sequences or fragments of mononucleosomal size obtained from sonication and MNase digestion assays of nucleosome-free yeast DNA. Each curve shows the number of words whose ranks are separated by a given distance or less in the sonication and MNase digestion vs. nucleosomal fits. ρ is the Spearman rank correlation coefficient. (*B*) Same as Fig. 2*A* except the dinucleotide frequencies are from mononucleosome-size DNA sequences (defined by >5 sequence reads) from yeast genomic DNA digested by MNase in the absence of nucleosomes.

leading to enrichment in nucleosome-positioning sequences even in the absence of histones.

Discussion

Although nucleosome positioning has been extensively studied with high-throughput methods (5, 14, 15, 18, 21, 25, 30, 33, 34), the origin of intrinsic histone-DNA sequence specificity and its contribution to the structure of in vivo chromatin remain controversial. We have developed a biophysical approach to inferring nucleosome energies and occupancies directly from high-throughput sequencing data. The effects of steric exclusion are rigorously separated from intrinsic histone-DNA interactions under the assumption that nucleosomes form a one-dimensional array in which there are no nucleosome-nucleosome interactions besides nearest-neighbor steric hindrance. This assumption amounts to neglecting intrinsic structure of the chromatin fiber which is believed to impose "quantized" linker lengths (27, 28). Furthermore, we assume that the one-dimensional nucleosome array is in thermodynamic equilibrium, with individual nucleosome positions corresponding to the lowest free energy state of the entire array.

We find that most nucleosomes mapped in vitro are not sequence specific. However, well-positioned nucleosomes tend to occupy G:C-enriched and A:T-depleted DNA segments in *S. cerevisiae* (Fig. 2 *A* and *B*). A:T and G:C dinucleotide content changes sharply across the nucleosome boundary and is thus highly predictive of nucleosome positions. More complex models that take rotational positioning into account do not yield significantly improved predictions (Table S1), indicating that G:C content is an essential nucleosome-positioning determinant. $N = 2$ position-independent models trained on Zhang et al. and Kaplan et al. in vitro maps yield very similar results (Table S1 and Dataset S1), despite the rather low correlation ($r = 0.69$) between the datasets themselves.

Surprisingly, models trained on DNA from nucleosome-free control experiments can be used to predict nucleosome occupancies (Fig. 4*A* and Table S1). It is possible that MNase-based nucleosome maps are biased to some extent by the sequence specificity of MNase exonuclease activity (although we cannot rule out coincidence), whereas similarities between nucleosome-positioning sequences and the sonication control appear to be coincidental. MNase- and sonication-free nucleosome-positioning maps are required to fully resolve the issue of experimental bias.

In summary, nucleosome sequence preferences can be captured using a simple physical model based on dinucleotide content. Promoter regions are unfavorable for nucleosome formation, while +1 nucleosomes have lower energies, helping define nucleosome array boundaries. Nonetheless, sequence preferences alone cannot explain why nucleosomes are ordered into well-defined arrays in vivo (Fig. S7). Similar nucleosome-positioning signals can be extracted from in vitro and in vivo chromatin (Fig. S9), showing that nucleosomes tend to occupy thermodynamically favorable positions in living cells (5).

Materials and Methods

Parallel Sequencing and Mapping of Control and Nucleosome Data. Genomic DNA from *S. cerevisiae* and *E. coli* was purified using Qiagen genomic tip 500/G, and mixed in a 3:1 mass ratio. Part of the mixture was treated with MNase to yield a small average fragment size (<300 bp), and DNA fragments of approximately 150 bp were purified by excision from an agarose gel. A second fraction of the yeast/bacterial DNA mixture was subjected to sonication in a Misonix water-bath instrument to yield an average fragment size of 150 bp, as described earlier (25). Mononucleosome-size DNA fragments were sequenced using Illumina Genome Analyzer, and mapped to the *S. cerevisiae* genome (SGD April 2008 build) and to the *E. coli* K12 genome (U00096), allowing up to two mismatches per read.

We have taken a map of nucleosomes assembled in vitro on the same mixture of yeast and bacterial DNA from our previous study (25). In addition, Kaplan et al. provided two replicates for nucleosomes reconstituted in vitro on yeast genomic DNA, and six replicates (two with and four without cross-linking) for nucleosomes from log-phase yeast cells grown in YPD medium (5). We have combined the replicates separately in each of the three categories using sequence read coordinates provided by the authors. Finally, coordinates of *C. elegans* nucleosomes from mixed-stage, wild-type (N2) cells are from Valouev et al. (30).

Preprocessing of Nucleosome Sequence Reads. We assume that the coordinate of each mapped read gives the actual nucleosome location. We extend all mapped reads to the 147 bp canonical nucleosome length and combine reads from both strands (*SI Text*). This procedure yields the number of nucleosomes that start at each genomic bp (the sequence read profile; Fig. S1*A*), as well as the number of nucleosomes that cover a given bp (the nucleosome coverage profile). We control for sequencing and mapping artifacts by removing regions with anomalously high and low nucleosome coverage from further consideration (*SI Text*).

Next we smooth the sequence read and nucleosome coverage profiles by replacing the number of nucleosomes starting at each bp with a Gaussian centered on that bp (14, 15). The area of the Gaussian is equal to the number of sequence reads starting at that position, and its σ is set to either 2 or 20. Gaussian smoothing is necessary because current levels of sequence read coverage lead to large deviations in the number of nucleosomes located

at neighboring bps, contrary to the expectation that such nucleosomes should have very similar binding affinities because they occupy nearly identical sites (11). The effect of Gaussian smoothing can be seen in Fig. S10.

Finally, we normalize the sequence read and nucleosome coverage profiles by the highest value of nucleosome coverage on the chromosome. We interpret the resulting normalized profiles as the probability to start a nucleosome at a given bp (the nucleosome probability profile) and the probability that a given bp is covered by any nucleosome (the nucleosome occupancy profile; Fig. S1*B*).

Prediction of Nucleosome Energetics from High-Throughput Sequencing Maps. We derive nucleosome formation energies directly from the smoothed probability and occupancy profiles, under the assumption that observed nucleosome positions are affected solely by intrinsic histone-DNA interactions and steric exclusion (*SI Text*):

$$\frac{E_i-\mu}{k_BT}=\log\frac{1-O_i+P_i}{P_i}+\sum_{j=i}^{i+146}\log\frac{1-O_j}{1-O_j+P_j},\quad i=1,\ldots,L-146. \qquad [1]$$

Here E_i is the Percus energy at bp i, μ is the chemical potential of histone octamers, k_BT is the product of the Boltzmann constant and room temperature, L is the number of bps in the DNA segment, P_i is the probability to start a nucleosome at bp i, and O_i is the nucleosome occupancy of bp i ($O_i=\sum_{j=i-146}^{i}P_j$).

We establish the degree of correlation between Percus energies and sequence features found in nucleosomal and linker DNA by fitting them to one of four sequence-specific models (Fig. S1*C*). The position-independent model of order N is given by:

$$\frac{E_i-\mu}{k_BT}=\sum_{n=1}^{N}\sum_{\{\alpha_1\ldots\alpha_n\}}^{4^n}n^i_{\alpha_1\ldots\alpha_n}\epsilon_{\alpha_1\ldots\alpha_n}+\epsilon^0+r_i, \qquad [2]$$

where N is the maximum word length, ϵ^0 is the sequence-independent offset, and $n^i_{\alpha_1\ldots\alpha_n}$ is the number of times a word of length n with sequence $\alpha_1\ldots\alpha_n$ [$\alpha=\{A,C,G,T\}$] was found within the nucleosome that started at bp i. $\epsilon_{\alpha_1\ldots\alpha_n}$ are word energies, and r_i is the residual at bp i. The word energies are constrained by $\sum_{\alpha_i}\epsilon_{\alpha_1\ldots\alpha_n}=0$, $\forall\, i=1\ldots n$, which leaves 3^n independent words of length n (the constraints are introduced into Eq. **2** prior to the fit). We exclude all words that extend into three terminal bps on each end of the 147 bp nucleosomal site from our counts.

The spatially resolved model is defined by:

$$\frac{E_i-\mu}{k_BT}=\sum_{j=i+3}^{i+143}\epsilon_{\alpha_j\alpha_{j+1}}+\sum_{j=i+3}^{i+144}\epsilon_{\alpha_j}+\epsilon^0+r_i, \qquad [3]$$

where the mono- and dinucleotide energies are constrained as above at each position within the nucleosomal site. The three-region model and the periodic model are described in the *SI Text*. We use Gaussian smoothing with $\sigma=20$ for position-independent and three-region models and $\sigma=2$ for spatially resolved and periodic models.

Eqs. **2** and **3** define linear models which we fit against Percus energies using the *lm* function from R statistical software (http://www.r-project.org) (Fig. S1*C*). For computational reasons the genome is divided into several segments of equal size and a separate model is trained on each segment (Fig. S11). The final energy of each word is the average over all models. To restore the dynamic range of the fitted energies, we rescale the variance of the fitted energies to match the Percus energies on which they were trained. We rescale each chromosome separately. Finally, we predict nucleosome probabilities and occupancies from fitted energies using a standard recursive algorithm (Fig. S1*D* and *SI Text*) (22). Our predictions, data, and software are available on the Nucleosome Explorer website, http://nucleosome.rutgers.edu. DNA sequencing data has been deposited on Gene Expression Omnibus with the accession number of GSE23712.

ACKNOWLEDGMENTS. We thank Jerry K. Percus for helpful discussions. This research was supported by National Institutes of Health (HG 004708 to A.V.M. and GM 30186 to K.S.). A.V.M. acknowledges support from an Alfred P. Sloan Research Fellowship.

1. van Holde KE (1989) *Chromatin* (Springer, New York).
2. Richmond TJ, Davey CA (2003) The structure of DNA in the nucleosome core. *Nature* 423:145–150.
3. Felsenfeld G, Groudine M (2003) Controlling the double helix. *Nature* 421:448–453.
4. Jenuwein T, Allis C (2001) Translating the histone code. *Science* 293:1074–1080.
5. Kaplan N, et al. (2009) The DNA-encoded nucleosome organization of a eukaryotic genome. *Nature* 458:362–366.
6. Sekinger EA, Moqtaderi Z, Struhl K (2005) Intrinsic histone-DNA interactions and low nucleosome density are important for preferential accessibility of promoter regions in yeast. *Mol Cell* 18:735–748.
7. Becker PB, Hörz W (2002) ATP-dependent nucleosome remodeling. *Annu Rev Biochem* 71:247–273.
8. Deckert J, Struhl K (2001) Histone acetylation at promoters is differentially affected by activators and repressors. *Mol Cell Biol* 21:2726–2735.
9. Adams CC, Workman JL (1995) Binding of disparate transcriptional activators to nucleosomal DNA is inherently cooperative. *Mol Cell Biol* 15:1405–1421.
10. Miller JA, Widom J (2003) Collaborative competition mechanism for gene activation in vivo. *Mol Cell Biol* 23:1623–1632.
11. Segal E, et al. (2006) A genomic code for nucleosome positioning. *Nature* 442:772–778.
12. Kornberg RD, Stryer L (1988) Statistical distributions of nucleosomes: nonrandom locations by a stochastic mechanism. *Nucleic Acids Res* 16:6677–6690.
13. Fedor MJ, Lue NF, Kornberg RD (1988) Statistical positioning of nucleosomes by specific protein-binding to an upstream activating sequence in yeast. *J Mol Biol* 204:109–127.
14. Mavrich TN, et al. (2008) Nucleosome organization in the Drosophila genome. *Nature* 453:358–362.
15. Mavrich TN, et al. (2008) A barrier nucleosome model for statistical positioning of nucleosomes throughout the yeast genome. *Genome Res* 18:1073–1083.
16. Widom J (2001) Role of DNA sequence in nucleosome stability and dynamics. *Q Rev Biophys* 34:269–324.
17. Ioshikhes IP, Albert I, Zanton SJ, Pugh BF (2006) Nucleosome positions predicted through comparative genomics. *Nat Genet* 38:1210–1215.
18. Field Y, et al. (2008) Distinct modes of regulation by chromatin encoded through nucleosome positioning signals. *PLoS Comput Biol* 4(11):e1000216.
19. Yuan GC, Liu JS (2008) Genomic sequence is highly predictive of local nucleosome depletion. *PLoS Comput Biol* 4(1):e13.
20. Peckham HE, et al. (2007) Nucleosome positioning signals in genomic DNA. *Genome Res* 17:1170–1177.
21. Lee W, et al. (2007) A high-resolution atlas of nucleosome occupancy in yeast. *Nat Genet* 39:1235–1244.
22. Morozov AV, et al. (2009) Using DNA mechanics to predict in vitro nucleosome positions and formation energies. *Nucleic Acids Res* 37:4707–4722.
23. Miele V, Vaillant C, d'Aubenton Carafa Y, Thermes C, Grange T (2008) DNA physical properties determine nucleosome occupancy from yeast to fly. *Nucleic Acids Res* 36:3746–3756.
24. Tolstorukov MY, Colasanti AV, McCandlish DM, Olson WK, Zhurkin VB (2007) A novel roll-and-slide mechanism of DNA folding in chromatin: implications for nucleosome positioning. *J Mol Biol* 371:725–738.
25. Zhang Y, et al. (2009) Intrinsic histone-DNA interactions are not the major determinant of nucleosome positions in vivo. *Nature Struct Mol Biol* 16:847–852.
26. Percus JK (1976) Equilibrium state of a classical fluid of hard rods in an external field. *J Stat Phys* 15:505–511.
27. Ulanovsky LE, Trifonov EN (1986) *Biomolecular Stereodynamics III* (Adenine Press, New York), pp 35–44.
28. Wang JP, et al. (2008) Preferentially quantized linker DNA lengths in *Saccharomyces cerevisiae*. *PLoS Comput Biol* 4(9):e1000175.
29. Tillo D, Hughes TR (2009) G+C content dominates intrinsic nucleosome occupancy. *BMC Bioinformatics* 10:442.
30. Valouev A, et al. (2008) A high-resolution, nucleosome position map of *C. elegans* reveals a lack of universal sequence-dictated positioning. *Genome Res* 18:1051–1063.
31. Wingert L, Von Hippel PH (1968) The conformation dependent hydrolysis of DNA by micrococcal nuclease. *Biochim Biophys Acta* 157:114–126.
32. Hörz W, Altenburger W (1981) Sequence specific cleavage of DNA by micrococcal nuclease. *Nucleic Acids Res* 9:2643–2658.
33. Yuan GC, et al. (2005) Genome-scale identification of nucleosome positions in *S. cerevisiae*. *Science* 309:626–630.
34. Zawadzki KA, Morozov AV, Broach JR (2009) Chromatin-dependent transcription factor accessibility rather than nucleosome remodeling predominates during global transcriptional restructuring in *Saccharomyces cerevisiae*. *Mol Biol Cell* 20:3503–3513.

Supporting Information

Locke et al. 10.1073/pnas.1003838107

SI Materials and Methods

Preprocessing High-Throughput Sequencing Data. ***Mapping sequence reads.*** We start from a collection of 25 bp-long Solexa sequence reads uniquely mapped onto the yeast genome with no more than two mismatches (1). Each read is mapped onto either the forward (5′) or the reverse (3′) strand. For sequence reads mapped onto the forward (5′) strand, we interpret the first base of a read as the start position of a nucleosome with the canonical length of 147 bp. For sequence reads mapped onto the reverse (3′) strand, we interpret the last base of the read as the end position of a 147 bp nucleosome. Thus we create a "sequence read profile," a table which shows the number of nucleosomes starting at each genomic bp. This table is used to create a "read coverage profile" showing how many nucleosomes cover each genomic bp: the value of the read coverage profile at position i is equal to the sum over all reads located at positions $i-146\ldots i$.

Filtering sequence read profiles. We observe large gaps in our read profiles, possibly due to repetitive regions in the genome to which reads cannot be mapped uniquely, or to sequencing artifacts. We considered any stretch of ≥1,000 bp without mapped reads to be anomalous and excluded such regions from further analysis. We also find regions where the read coverage was uncharacteristically high. For instance, our in vitro nucleosome measurement for chromosome 12 has an average nucleosome coverage of ∼80 reads, but there is a small region near bp 460,000 covered with 5,000 reads. We exclude such regions according to the following procedure: For each chromosome, we find the average number of reads per bp. Next, for each bp we calculate the running average number of reads in a window extending 75 bp in each direction. If this running average is more than three times the chromosome-wide mean, we flag the region which extends out from the identified point in both directions until the running average equals the mean, and we remove this region from consideration. We then create a filter which marks the union of all excluded regions. Finally, each excluded region is extended 146 bp upstream so that there is no contribution to the Percus energy from filtered regions.

Normalizing sequence read profiles. Next we use the sequence read profile to create nucleosome probability and occupancy profiles. First, we set sequence read counts to zero inside all filtered regions. Second, we use a Gaussian smoothing algorithm that replaces the number of sequence reads at a given bp with a normal distribution centered at that bp. The Gaussian is chosen to have $\sigma = 2$ or 20 depending on subsequent modeling, and the area under the curve is equal to the number of sequence reads at that bp. The smoothed sequence read profile is then constructed as a superposition of all such Gaussians.

The smoothing procedure reflects a lack of bp precision in MNase digestion assays, which results in the uncertainty of the interpretation of sequence read coordinates as nucleosome start or end positions. In addition, because neighboring nucleosomes are expected to have similar binding affinities, collecting more sequence read data is assumed to result in a read profile that we approximate with the superposition of normal distributions centered on available reads.

We extend the smoothed read profile into a smoothed read coverage profile as described above, find the highest point $N_{\max}$ in the smoothed coverage profile and multiply the height of each point in the smoothed coverage profile and the smoothed read profile by $1/N_{\max}$ so that the maximum coverage is one. Each point in the smoothed sequence read profile may now be interpreted as the probability for a nucleosome to start at a given position, and the coverage may be interpreted as the probability for any nucleosome to occupy a given position. We refer to the scaled results as nucleosome probability and occupancy profiles, respectively.

Energetics of DNA-Binding One-Dimensional Particles of Finite Size. Consider particles of size a bp distributed along a DNA segment of length L bp. The particles can interact with DNA in a position-dependent manner and are also subject to steric exclusion (adjacent particles cannot overlap). A grand-canonical partition function for this system of DNA-bound particles is given by:

$$Z = \sum_{\text{conf}} e^{-[E(\text{conf})-\mu N(\text{conf})]}, \qquad \textbf{[S1]}$$

where conf denotes an arbitrary configuration of DNA-bound nonoverlapping particles, μ is the chemical potential, and $E(\text{conf})$ and $N(\text{conf})$ are the total DNA-binding energy and the number of particles in the current configuration (for simplicity we assume $k_B T = 1$, where k_B is the Boltzmann constant and T is the room temperature).

One can compute Z efficiently using a recursive relation (2):

$$\begin{aligned} Z_i^f &= Z_{i-1}^f + Z_{i-a}^f e^{-(E_{i-a+1}-\mu)}, \qquad i = a,\ldots,L \\ Z_{a-1}^f &= \ldots = Z_0^f = 1 \end{aligned} \qquad \textbf{[S2]}$$

which computes a set of partial partition functions in the forward direction. Likewise, partial partition functions can be computed in the reverse direction:

$$\begin{aligned} Z_i^r &= Z_{i+1}^r + Z_{i+a}^r e^{-(E_i-\mu)}, \qquad i = L-a+1,\ldots,1 \\ Z_{L-a+2}^r &= \ldots = Z_{L+1}^r = 1. \end{aligned} \qquad \textbf{[S3]}$$

Note that $Z_L^f = Z_1^r = Z$ by construction. Furthermore, the probability of starting a particle at position i is given by:

$$P_i = \frac{Z_{i-1}^f e^{-(E_i-\mu)} Z_{i+a}^r}{Z}, \qquad i = 1,\ldots,L-a+1. \qquad \textbf{[S4]}$$

Intuitively, Eq. **S4** is a partition function for all configurations in which a particle is bound at position i (occupying positions i through $i+a-1$), divided by the partition function for all possible configurations. Using Eqs. **S2**–**S4** we obtain:

$$\begin{aligned} Z_i^f - Z_{i-1}^f &= P_{i-a+1} Z / Z_{i+1}^r, \qquad i = a,\ldots,L \\ Z_{i+1}^r - Z_i^r &= -P_i Z / Z_{i-1}^f, \qquad i = L-a+1,\ldots,1. \end{aligned} \qquad \textbf{[S5]}$$

Note that both of these formulas can be extended to the $i = 1,\ldots,L$ range if we assume that $P_k = 0$, $k \notin [1, L-a+1]$. It is easy to show that $Z_i^f Z_{i+1}^r - Z_{i-1}^f Z_i^r = Z(P_{i-a+1} - P_i)$. This expression has the form of a complete differential and thus can be iterated as follows:

$$Z_L^f Z_{L+1}^r - Z_{i-1}^f Z_i^r = Z \sum_{j=i}^{L} (P_{j-a+1} - P_j), \qquad \textbf{[S6]}$$

yielding

$$Z^f_{i-1}Z^r_i = Z\left(1 - \sum_{j=i-a+1}^{i-1} P_j\right), \qquad i = 1,\ldots,L \qquad \textbf{[S7]}$$

Using Eqs. **S3**, **S4**, and **S7** we get:

$$Z^r_{i+1} = Z^r_i\left(1 - \frac{P_i}{1 - \sum_{j=i-a+1}^{i-1} P_j}\right). \qquad \textbf{[S8]}$$

Introducing $O_i = \sum_{j=i-a+1}^{i} P_j$—the probability that position i is covered by any particle regardless of its starting position (also called the particle occupancy), we see that:

$$Z^r_{i+1} = Z^r_i\left(1 - \frac{P_i}{1 - O_i + P_i}\right). \qquad \textbf{[S9]}$$

Using Eq. **S9** recursively (until $Z^r_{L+1} = 1$ is reached on the left-hand side), we obtain an explicit expression for Z^r_i:

$$Z^r_i = \prod_{j=i}^{L}\left(1 - \frac{P_j}{1 - O_j + P_j}\right)^{-1}, \qquad i = 1,\ldots,L. \qquad \textbf{[S10]}$$

Likewise, using Eqs. **S2**, **S4**, and **S7** together with $Z^f_0 = 1$ we get:

$$Z^f_i = \prod_{j=1}^{i}\left(1 - \frac{P_{j-a+1}}{1 - O_j + P_{j-a+1}}\right)^{-1}, \qquad i = 1,\ldots,L. \qquad \textbf{[S11]}$$

Eqs. **S10** and **S11** are explicit expressions for forward and reverse partial partition functions in terms of particle probabilities and occupancies. Note that $Z^r_1 = Z^f_L = Z$ still holds, with Eqs. **S10** and **S11** providing alternative expressions for the partition function in this limit. Inserting Eqs. **S10** and **S11** into Eq. **S4** and using Eq. **S7** to express Z^f_{i-1} in terms of Z^r_i leads to the desired expression for the DNA-binding energy of the particle at position i:

$$E_i - \mu = \log\frac{1 - O_i + P_i}{P_i} + \sum_{j=i}^{i+a-1} \log\frac{1 - O_j}{1 - O_j + P_j}, \quad i = 1,\ldots,L - a + 1. \qquad \textbf{[S12]}$$

Alternatively, we can use Eq. **S7** to express Z^r_{i+a} in terms of Z^f_{i+a-1}, leading to an equivalent expression for the DNA-binding energy:

$$E_i - \mu = \log\frac{1 - O_{i+a-1} + P_i}{P_i} + \sum_{j=i-a+1}^{i} \log\frac{1 - O_{j+a-1}}{1 - O_{j+a-1} + P_j}, \quad i = 1,\ldots,L - a + 1. \qquad \textbf{[S13]}$$

Hierarchical Models of Nucleosome Energetics. We have created hierarchical models of nucleosome energetics which assign nonzero energies to nucleotide words of length N only if the nucleosome energies cannot be explained using nucleotide words of lengths $1\ldots N-1$. The hierarchy is implemented through constraints on word energies:

$$\sum_{\alpha_i} \epsilon_{\alpha_1\ldots\alpha_N} = 0, \qquad \forall i = 1\ldots N. \qquad \textbf{[S14]}$$

Here $\epsilon_{\alpha_1\ldots\alpha_N}$ is the energy of the word of length N with nucleotides $\alpha_1\ldots\alpha_N$ at positions $1\ldots N$.

With these constraints and the $\{A,C,G,T\}$ alphabet there are 3^N independent parameters describing energetics of words of length N. For example, for $N = 1$ we can choose $\{\epsilon_A,\epsilon_G,\epsilon_T\}$ to be independent, while ϵ_C is fixed by the constraint: $\epsilon_C = -(\epsilon_A + \epsilon_G + \epsilon_T)$. For $N = 2$ there are nine independent parameters: $\{\epsilon_{AA},\epsilon_{AG},\epsilon_{AT},\epsilon_{GA},\epsilon_{GG},\epsilon_{GT},\epsilon_{TA},\epsilon_{TG},\epsilon_{TT}\}$, while the other seven dinucleotide energies can be expressed through these using Eq. **S14**. The remaining seven degrees of freedom are described by the lower order terms: six ϵ_α's (three for each position in the dinucleotide) and the total offset ϵ^0.

In general, D^N degrees of freedom associated with words of length N drawn from an alphabet of size D can be described using constrained energies:

$$D^N = (D-1)^N + \binom{N}{1}(D-1)^{N-1} + \cdots + \binom{N}{N}(D-1)^0, \qquad \textbf{[S15]}$$

where each term on the right describes the total number of constrained energies of order $(N,\ldots,0)$, computed as a product of the number of constrained energies at each possible position within the longer word, and the number of such positions. Note that the zeroth order term is simply the total offset ϵ^0. Furthermore, shorter words comprised of nonconsecutive nucleotides are included in the expansion. If we set the energies of all nonconsecutive words to zero, the total energy of a word of length N can be written as:

$$\epsilon'_{\alpha_1\ldots\alpha_N} = \sum_{n=1}^{N}\sum_{j=1}^{N-n+1} \epsilon_{\alpha_j\ldots\alpha_{j+n-1}} + \epsilon^0. \qquad \textbf{[S16]}$$

Note that here and below we set $\mu = 0$ for simplicity. Although a set of constrained energies of order $0,\ldots,N$ on the right-hand side of Eq. **S16** has fewer degrees of freedom than a set of unconstrained energies of order N, it provides the most complete description involving consecutive nucleotide words, and forms a basis of nucleosome models that have been further simplified by equating energies of words that occur at different positions within the nucleosomal site. Furthermore, because dinucleotides are too short to contain nonconsecutive motifs, Eq. **S16** entails no loss of degrees of freedom for $N = 2$.

Sequence-Specific Models of Nucleosome Energetics. Eq. **S12** can be used to convert nucleosome probabilities and occupancies obtained from high-throughput sequencing data into histone-DNA interaction energies for each position i along the DNA, under the assumption that steric exclusion and specific interactions with DNA are the only factors that affect nucleosome positions in vitro. In order to understand which DNA sequence features explain the observed energy profile, we carried out linear fits of genome-wide Percus energies (Eq. **S12**) to four sequence-specific models. Some models were designed to focus on the ~10–11 bp periodic distributions of sequence motifs, while others captured nucleosome-wide sequence signals such as motif enrichment and depletion in nucleosome-covered sequences.

Spatially resolved model. In terms of unconstrained energies, the spatially resolved model is defined as:

$$E(S) = \sum_{i=I_1}^{I_2-1} \epsilon'_{\alpha_i\alpha_{i+1}}, \qquad \textbf{[S17]}$$

where $E(S)$ is the sequence-specific part of the Percus energy of a 147 bp-long sequence S, $\epsilon'_{\alpha_i\alpha_{i+1}}$ is the energy of the dinucleotide with bases α_i and α_{i+1} at positions i and $i+1$ respectively, and the

sum runs from $I_1 \geq 1$ to $I_2 \leq 147$ in the nucleosomal site. To minimize edge effects, we typically exclude 3 bps from each end of the nucleosome, setting $I_1 = 4$ and $I_2 = 144$.

Eq. **S17** can be rewritten as:

$$E(S) = \sum_{i=I_1}^{I_2-1} (\epsilon_{\alpha_i\alpha_{i+1}} + \bar{b}_{\alpha_i} + b_{\alpha_{i+1}}) + \epsilon^0, \qquad \textbf{[S18]}$$

where

$$\epsilon^0 = \frac{1}{D^2} \sum_{i=I_1}^{I_2-1} \sum_{\alpha,\beta=1}^{D} \epsilon'_{\alpha\beta} \equiv \sum_{i=I_1}^{I_2-1} \epsilon^0_{i,i+1},$$

$$\bar{b}_\alpha = \frac{1}{D} \sum_{\beta=1}^{D} (\epsilon'_{\alpha\beta} - \epsilon^0_{i,i+1}),$$

$$b_\beta = \frac{1}{D} \sum_{\alpha=1}^{D} (\epsilon'_{\alpha\beta} - \epsilon^0_{i,i+1}).$$

Note that $\sum_{\alpha=1}^{D} \epsilon_{\alpha\beta} = \sum_{\beta=1}^{D} \epsilon_{\alpha\beta} = 0$ by construction. Eq. **S18** is equivalent to the expansion in terms of constrained energies which is consistent with Eq. **S16**:

$$E(S) = \sum_{i=I_1}^{I_2-1} \epsilon_{\alpha_i\alpha_{i+1}} + \sum_{i=I_1}^{I_2} \epsilon_{\alpha_i} + \epsilon^0, \qquad \textbf{[S19]}$$

where $\epsilon_{\alpha_{I_1}} = \bar{b}_{\alpha_{I_1}}, \epsilon_{\alpha_{I_1+1}} = \bar{b}_{\alpha_{I_1+1}} + b_{\alpha_{I_1+1}}, \ldots, \epsilon_{\alpha_{I_2}} = b_{\alpha_{I_2}}$. Thus an unconstrained description of nucleosome energetics can be uniquely decomposed into a constrained description. However, the opposite is not true: for any p and q such that $p + q = 1$

$$\begin{aligned}
\epsilon'_{\alpha_{I_1}\alpha_{I_1+1}} &= \epsilon_{\alpha_{I_1}\alpha_{I_1+1}} + \epsilon_{\alpha_{I_1}} + q\epsilon_{\alpha_{I_1+1}}, \\
\epsilon'_{\alpha_i\alpha_{i+1}} &= \epsilon_{\alpha_i\alpha_{i+1}} + p\epsilon_{\alpha_i} + q\epsilon_{\alpha_{i+1}}, \qquad I_1 < i < I_2 - 1 \\
\epsilon'_{\alpha_{I_2-1}\alpha_{I_2}} &= \epsilon_{\alpha_{I_2-1}\alpha_{I_2}} + p\epsilon_{\alpha_{I_2-1}} + \epsilon_{\alpha_{I_2}}
\end{aligned}$$

are equally valid reconstructions that leave $E(S)$ unchanged. In this paper we use $p = 1$, $q = 0$ to compute unconstrained dinucleotide energies from constrained ones.

Position-independent model. This model assigns the same energy to a given word within the nucleosome, regardless of its position in the site. Thus the position-independent model of order N is given by:

$$E(S) = \sum_{n=1}^{N} \sum_{\{\alpha_1 \ldots \alpha_n\}}^{4^n} n_{\alpha_1 \ldots \alpha_n} \epsilon_{\alpha_1 \ldots \alpha_n} + \epsilon^0, \qquad \textbf{[S20]}$$

where the outer sum is over word lengths, the inner sum is over all distinct words of length n, $n_{\alpha_1 \ldots \alpha_n}$ is the number of words with the nucleotides $\alpha_1 \ldots \alpha_n$ at positions $1 \ldots n$, and $\epsilon_{\alpha_1 \ldots \alpha_n}$ are the word energies that are either explicitly fit or given by the constraints (Eq. **S14**). As in the spatially resolved model, the words are counted from bp $I_1 = 4$ to bp $I_2 = 144$, excluding 3 bp from each end of the site. The words are not allowed to extend outside this region. Note that both in this model and in the two partially position-dependent models described below there is no one-to-one correspondence between constrained models utilizing words of order $1 \ldots N$ and their unconstrained counterparts utilizing words of order N—the former require fewer fitting parameters.

Three-region model. This model refines the position-independent model by dividing the 141 bp nucleosome site into three regions of equal length. Word energies are fitted separately inside each region. The total energy of sequence S is then given by:

$$E(S) = \sum_{r=1}^{3} \sum_{n=1}^{N} \sum_{\{\alpha_1 \ldots \alpha_n\}}^{4^n} n^r_{\alpha_1 \ldots \alpha_n} \epsilon^r_{\alpha_1 \ldots \alpha_n} + \epsilon^0, \qquad \textbf{[S21]}$$

where r refers to a particular 47 bp region.

Periodic model. This model enforces DNA helical twist periodicity by equating the energies of words separated by a multiple of 10 bp. To reduce the number of fitting parameters, we also grouped energies of words at positions 1…10 into five distinct bins. Thus e.g., the word AGT starting at position 1 within the nucleosome site would have the same energy as the word AGT starting at positions 11,21,31… as well as positions 2,12,22…, whereas the energy of the same word starting at positions 3 and 4 is grouped into a different bin. The total energy is then computed as:

$$E(S) = \sum_{b=1}^{5} \sum_{n=1}^{N} \sum_{\{\alpha_1 \ldots \alpha_n\}}^{4^n} n^b_{\alpha_1 \ldots \alpha_n} \epsilon^r_{\alpha_1 \ldots \alpha_n} + \epsilon^0, \qquad \textbf{[S22]}$$

where b is the bin index used to group motifs separated by the helical twist as described above. As before, all words overlapping with the 3 bp edge regions are excluded from the counts.

Other Supporting Information Files

Table of correlation coefficients between predicted or observed occupancy profiles on the yeast genome. All observed profiles have been filtered for abnormally high- and low-density regions as described in *SI Text*. Each correlation coefficient is computed only for those base pairs that have not been filtered in either dataset. Note that predicted occupancies do not have filtered regions.

Dataset S1 (XLS)

1. Zhang Y, et al. (2009) Intrinsic histone-DNA interactions are not the major determinant of nucleosome positions in vivo. *Nature Struct. Mol. Biol.* 16:847–852.
2. Morozov AV, et al. (2009) Using DNA mechanics to predict in vitro nucleosome positions and formation energies. *Nucleic Acids Res.* 37:4707–4722.
3. Kaplan N, et al. (2009) The DNA-encoded nucleosome organization of a eukaryotic genome. *Nature* 458:362–366.
4. Valouev A, et al. (2008) A high-resolution, nucleosome position map of *C. elegans* reveals a lack of universal sequence-dictated positioning. *Genome Res.* 18:1051–1063.
5. Flaus A, Luger K, Tan S, Richmond T (1996) Mapping nucleosome position at single base-pair resolution by using site-directed hydroxyl radicals. *Proc Natl Acad Sci USA* 93:1370–1375.
6. Kassabov S, Henry N, Zofall M, Tsukiyama T, Bartholomew B (2002) High-resolution mapping of changes in histone-DNA contacts of nucleosomes remodeled by ISW2. *Mol Cell Biol.* 22:7524–7534.
7. Davey C, Pennings S, Reilly C, Meehan R, Allan J (2004) A determining influence for CpG dinucleotides on nucleosome positioning in vitro. *Nucl Acids Res* 32:4322–4331.
8. Lowary P, Widom J (1998) New DNA sequence rules for high-affinity binding to histone octamer and sequence-directed nucleosome positioning. *J Mol Biol* 276:19–42.
9. Nagalakshmi U, et al. (2008) The transcriptional landscape of the yeast genome defined by RNA sequencing. *Science* 320:1344–1349.

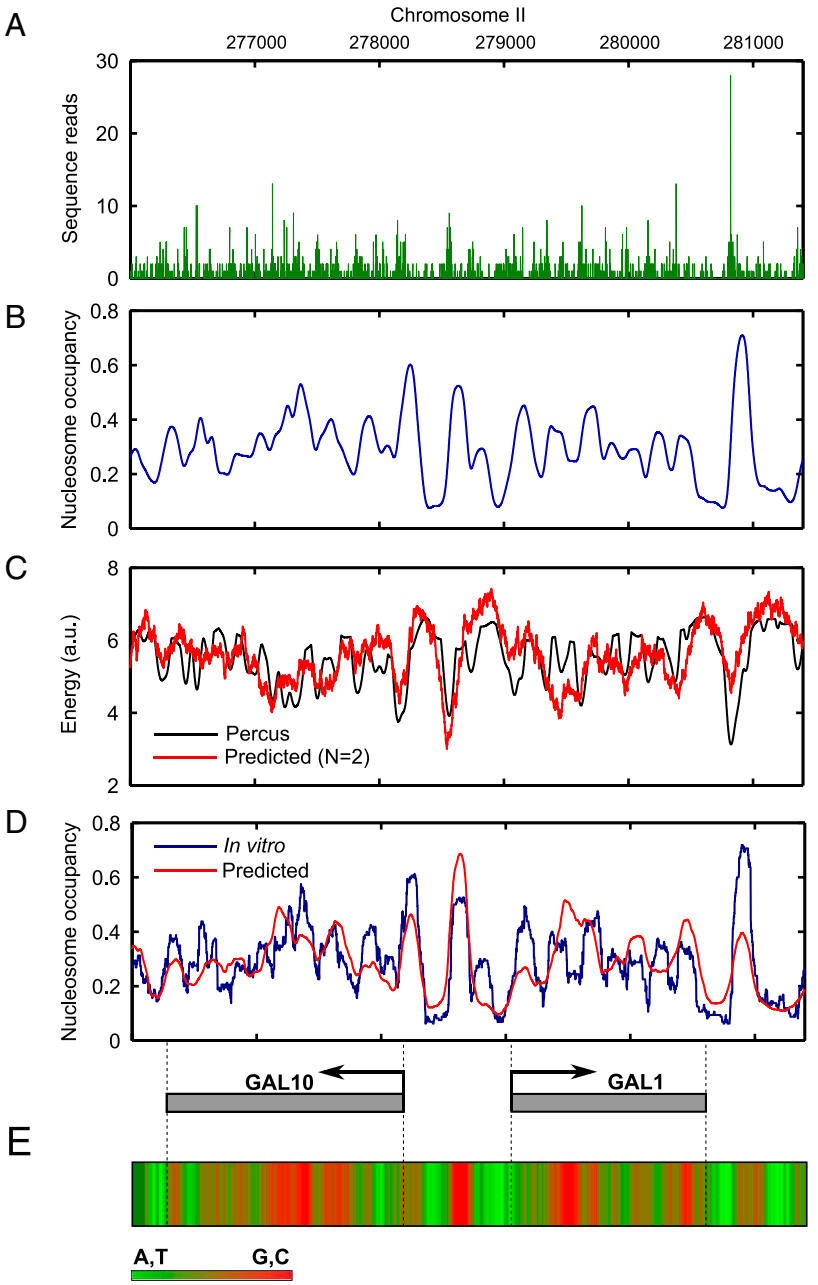

Fig. S1 Outline of the biophysical approach to nucleosome occupancy predictions: GAL1-10 *S. cerevisiae* locus. (*A*) Nucleosome starting positions mapped to the *GAL1-10* locus in the in vitro reconstitution experiment (25). (*B*) Nucleosome occupancy based on the nucleosome starting positions shown in (*A*) and smoothed with a $\sigma = 20$ Gaussian (see *SI Text*). (*C*) Percus energy inferred from the occupancy profile shown in (*B*), and a sequence-specific linear fit to an $N = 2$ position-independent model. (*D*) Nucleosome occupancy predicted using sequence-specific energies and compared with the experimental occupancy based on the nucleosome starting positions shown in (*A*) [same as (*B*) but without Gaussian smoothing]. (*E*) Nucleosomes are positioned over G:C-rich sequences: shown are nucleotide counts in the *GAL1-10* locus, smoothed with a 100 bp moving average.

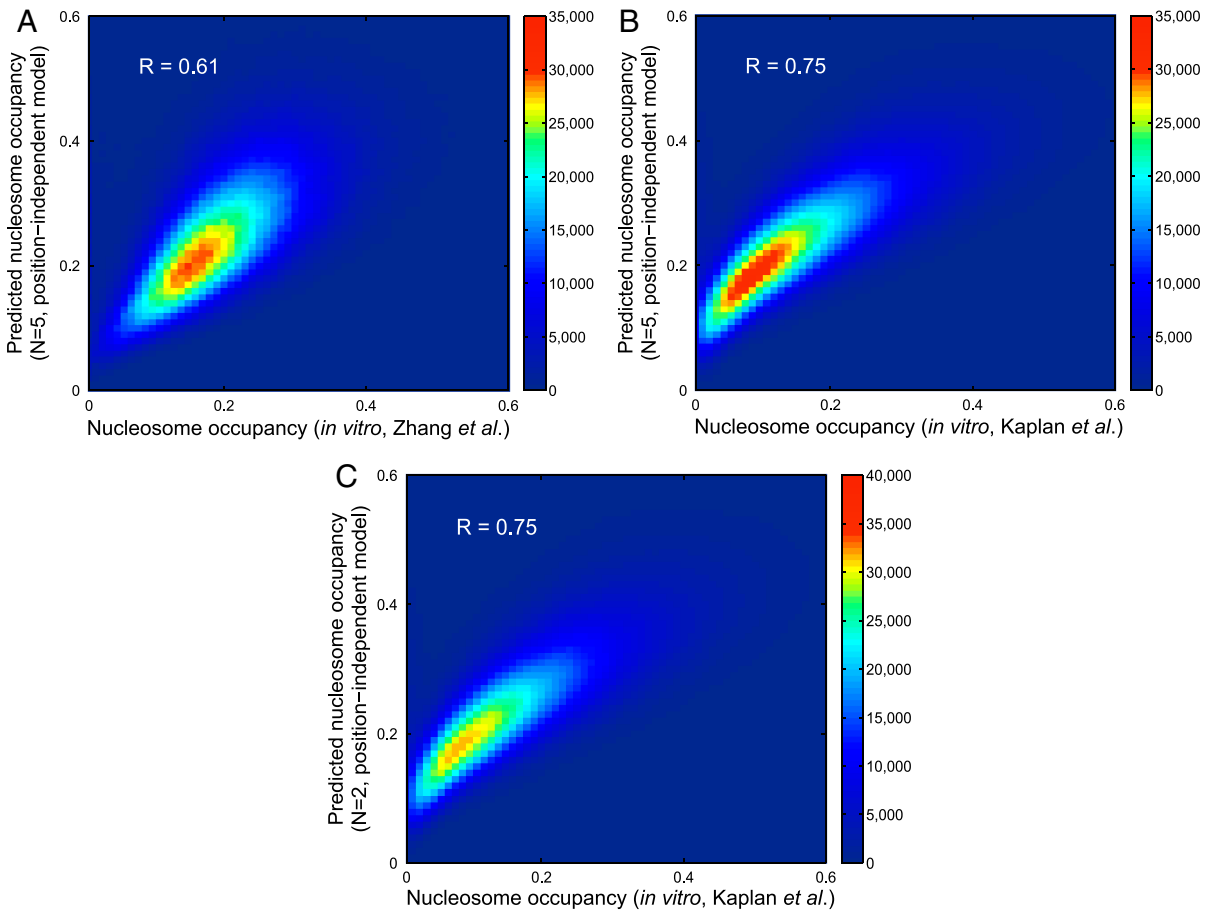

Fig. S2. Position-independent models explain in vitro nucleosome occupancy in *S. cerevisiae*. (*A*) Density scatter plot for the nucleosome occupancy at each genomic base pair (predicted with the $N = 5$ position-independent model) vs. in vitro occupancy observed by Zhang et al. (1). (*B*) Same as (*A*) except that in vitro occupancy is from Kaplan et al. (3). (*C*) Same as (*B*) but for the $N = 2$ position-independent model.

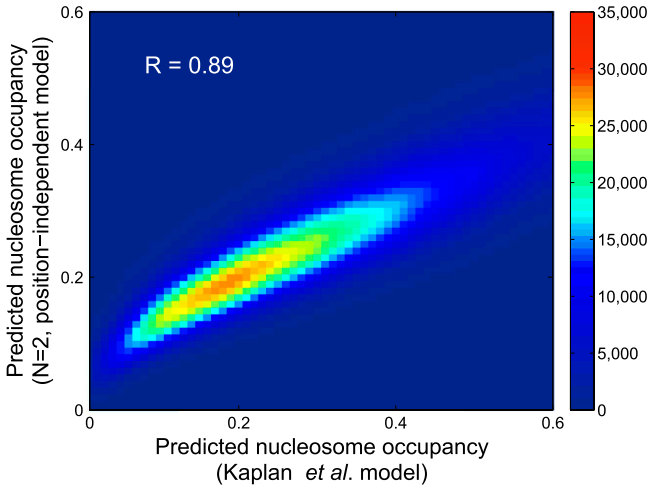

Fig. S3. Similar predictive power of the $N = 2$ position-independent model and a bioinformatics model based on periodic dinucleotide distributions and frequencies of 5 bp-long words (3). Density scatter plot for the nucleosome occupancy at each genomic base pair predicted with the $N = 2$ position-independent model vs. nucleosome occupancy predicted by Kaplan et al. (3).

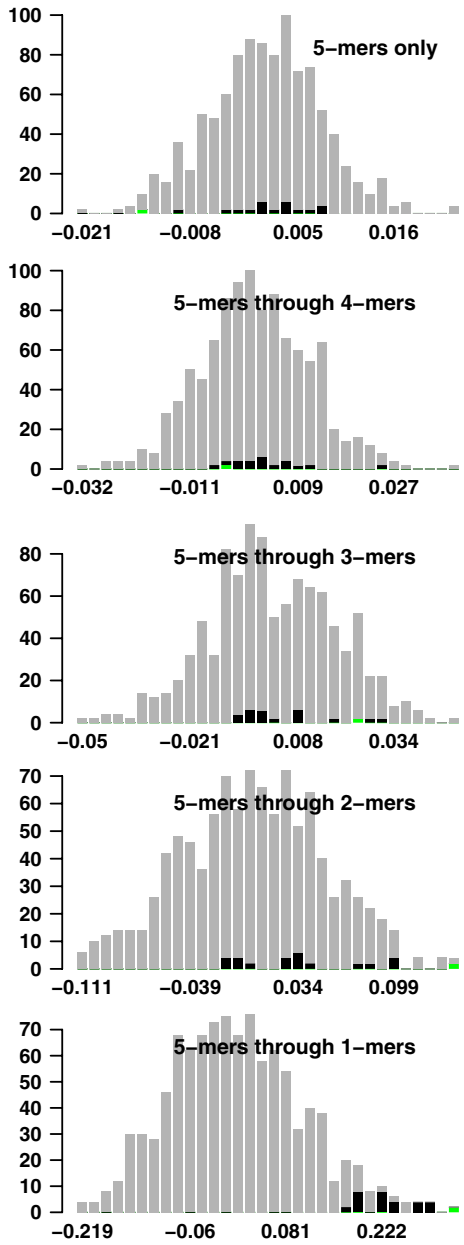

Fig. S4. Minor role of the higher-order contributions to the energies of 5 bp-long words. $N = 5$ position-independent model was trained on nucleosomes reconstituted in vitro on the yeast genome (1), yielding energies of all motifs of 1 through 5 bp in length. Energies of 5 bp-long words were then computed by summing contributions from a subset of shorter motifs: $E(S) = \sum_{n=L}^{5} \sum_{\{\alpha_1 \ldots \alpha_n\}}^{4^n} n_{\alpha_1 \ldots \alpha_n} \epsilon_{\alpha_1 \ldots \alpha_n}$, where $n_{\alpha_1 \ldots \alpha_n}$ is the number of times a given word was found in the 5 bp-long sequence S and $\epsilon_{\alpha_1 \ldots \alpha_n}$ is the fitted energy of that word. $L = 5 \ldots 1$ is the length of the shortest motif included into $E(S)$. Gray: all 5 bp-long words, black: A:T-containing words, green: the poly(dA:dT) tract (AAAAA).

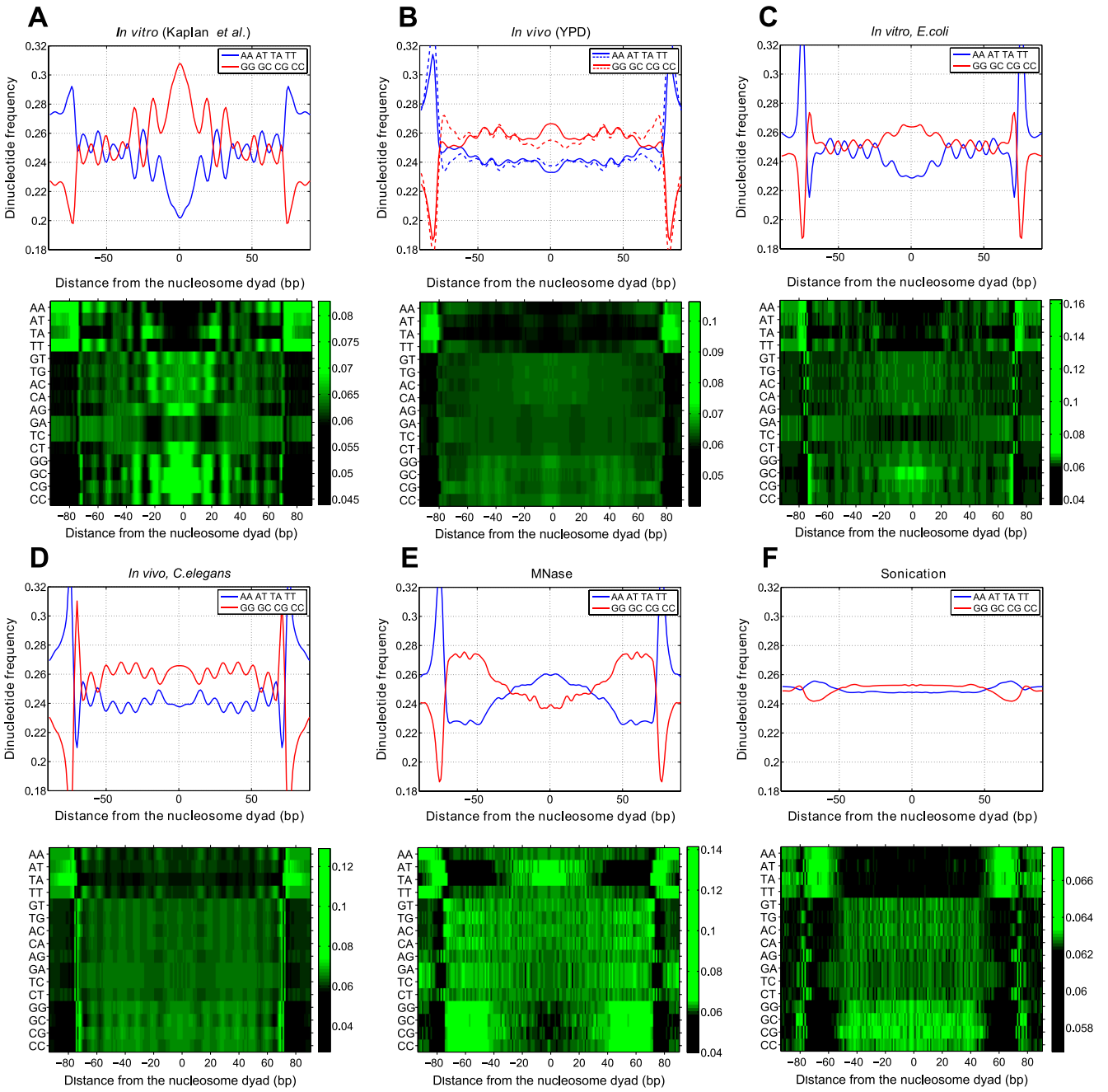

Fig. S5. Dinucleotide distributions in nucleosome and linker sequences. Upper: average relative frequencies of WW (AA, TT, AT, and TA) and SS (CC, GG, CG, and GC) dinucleotides at each position within the nucleosome are plotted with respect to the nucleosome dyad. The relative frequency of each dinucleotide is defined as its frequency at a given position divided by genome-wide frequency. All frequencies are smoothed using a 3 bp moving average. Lower: heat map of relative frequencies for each dinucleotide, plotted with respect to the nucleosome dyad. (*A*) Nucleosomes assembled in vitro on the yeast genome (defined by more than five sequence reads), from Kaplan et al. (3). (*B*) In vivo nucleosomes (defined by more than five sequence reads) from yeast cells grown in YPD medium (3). Upper: dashed lines—cross-linked nucleosomes, solid lines—no cross-linking. Lower: dinucleotide counts based on a combination of all YPD replicates. (*C*) Nucleosomes assembled in vitro on the *E. coli* genome (defined by more than one sequence read) (1). (*D*) In vivo nucleosomes (defined by more than three sequence reads) from *C. elegans* (4). (*E*) Relative dinucleotide frequencies in mononucleosome-size DNA sequences (defined by more than five sequence reads) from yeast genomic DNA digested by MNase in the absence of nucleosomes. (*F*) Same as (*E*) except mononucleosome-size DNA sequences (defined by more than one sequence read) were obtained by sonication.

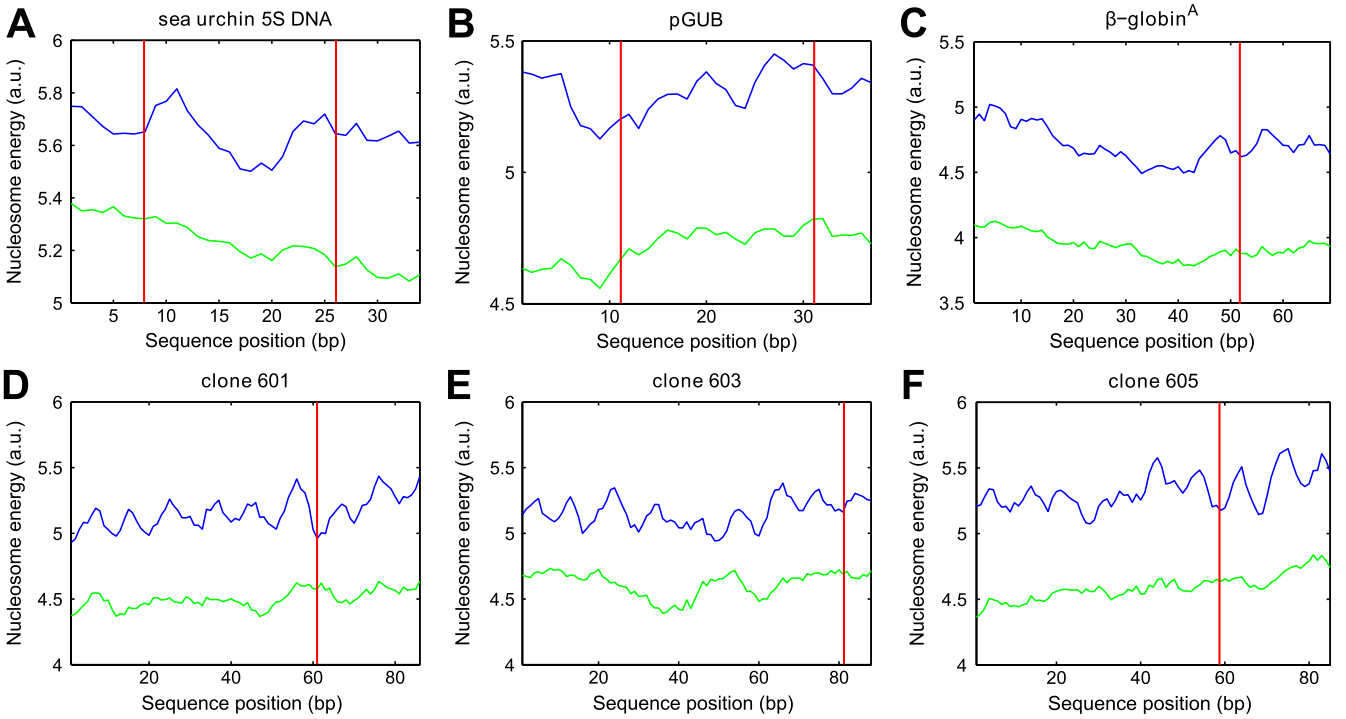

Fig. S6. Prediction of six nucleosome positions mapped in vitro at high resolution. Shown are nucleosome formation energies computed using the $N = 2$ position-independent model (green curves) and the spatially resolved model (blue curves). Vertical lines: known nucleosome starting positions, also listed in parentheses below. (*A*) The 180 bp sequence from the sea urchin 5S rRNA gene (bps 8, 26) (5). (*B*) The 183 bp sequence from the pGUB plasmid (bps 11, 31) (6). (*C*) The 215 bp fragment from the sequence of the chicken β-globin^A gene (bp 52) (7). (*D*, *E*, *F*) Synthetic high-affinity sequences (8): 601 (bp 61), 603 (bp 81), and 605 (bp 59).

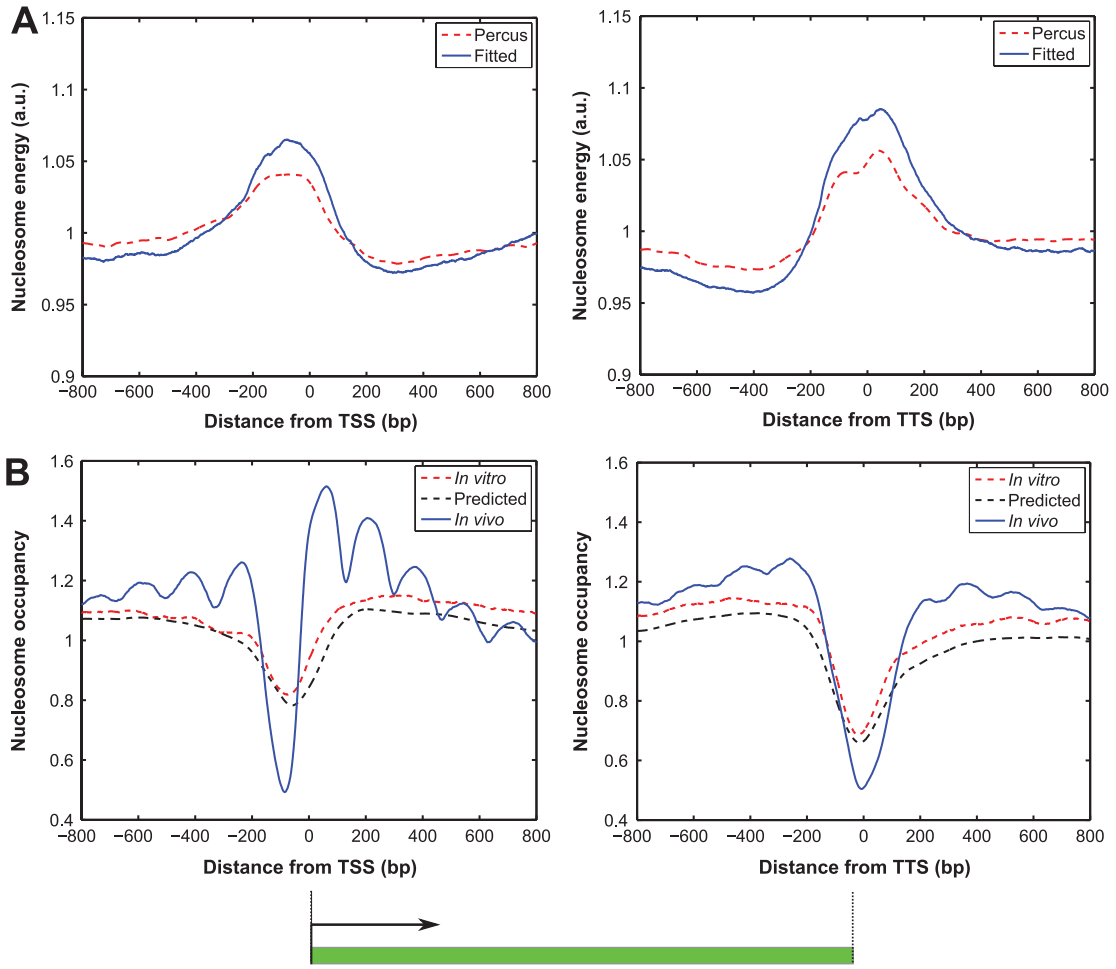

Fig. S7. Nucleosome energies and occupancies in the vicinity of transcription start and termination sites. (*A*) Percus energy (red) and the sequence-specific energy predicted using the $N = 2$ position-independent model (blue). The energies were inferred from nucleosomes positioned in vitro on the yeast genome (1), averaged over all genes for which transcript coordinates were available (9), and plotted with respect to the transcription start and termination sites (TSS and TTS, respectively). All energies were divided by the genome-wide average. (*B*) In vitro nucleosome occupancy (red) (1), in vivo nucleosome occupancy in YPD medium without cross-linking (blue) (3), and occupancy predicted using the $N = 2$ position-independent model (black). All occupancies were divided by the genome-wide average and plotted as described in (*A*).

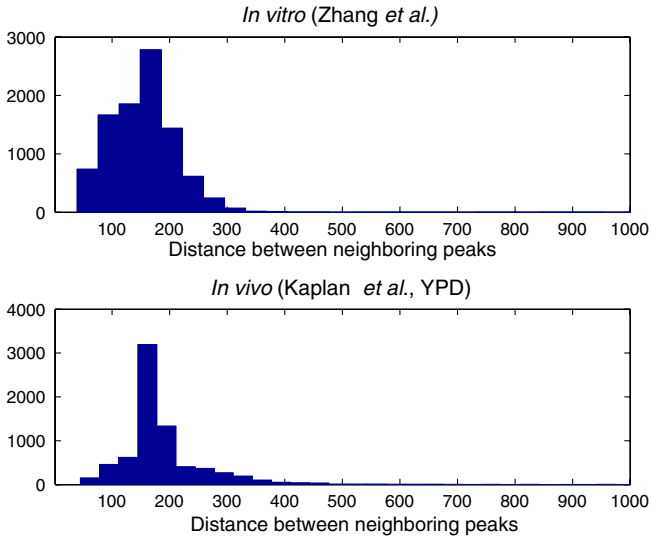

Fig. S8. Histogram of distances between neighboring peaks from in vitro and in vivo nucleosome sequence read profiles in *S. cerevisiae*. Mapped sequence reads were smoothed with a $\sigma = 20$ Gaussian. Neighboring peaks are defined by local maxima in the sequence read profile.

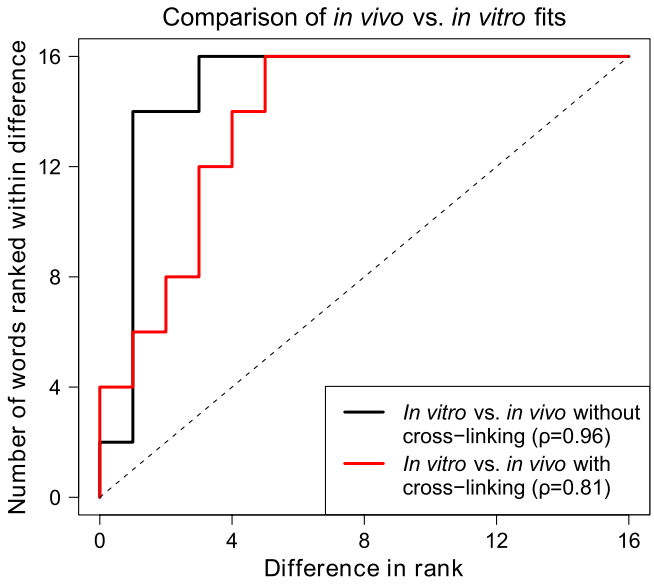

Fig. S9. Comparison of $N = 2$ position-independent models trained on in vitro and in vivo *S. cerevisiae* nucleosomes. Rank-order plots of energies of 2 bp words: the energy of each word is ranked using a position-independent model of order $N = 2$ trained on either in vivo (with and without cross-linking) or in vitro nucleosome positioning data. Each curve shows the number of words whose ranks are separated in the in vivo vs. in vitro fits by a given distance or less. ρ is the Spearman rank correlation coefficient.

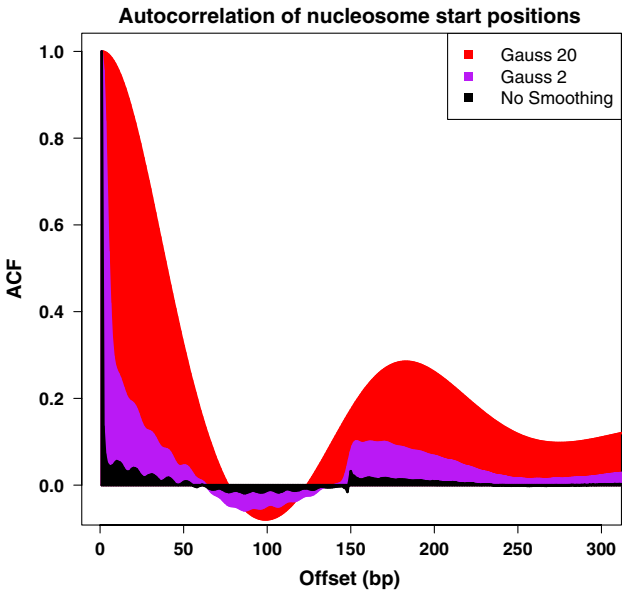

Fig. S10. Autocorrelation functions of nucleosome starting positions. Nucleosomes were assembled in vitro on the yeast genome (1). Black: original starting positions, violet: starting positions smoothed with a $\sigma = 2$ Gaussian, red: starting positions smoothed with a $\sigma = 20$ Gaussian (see *SI Text*).

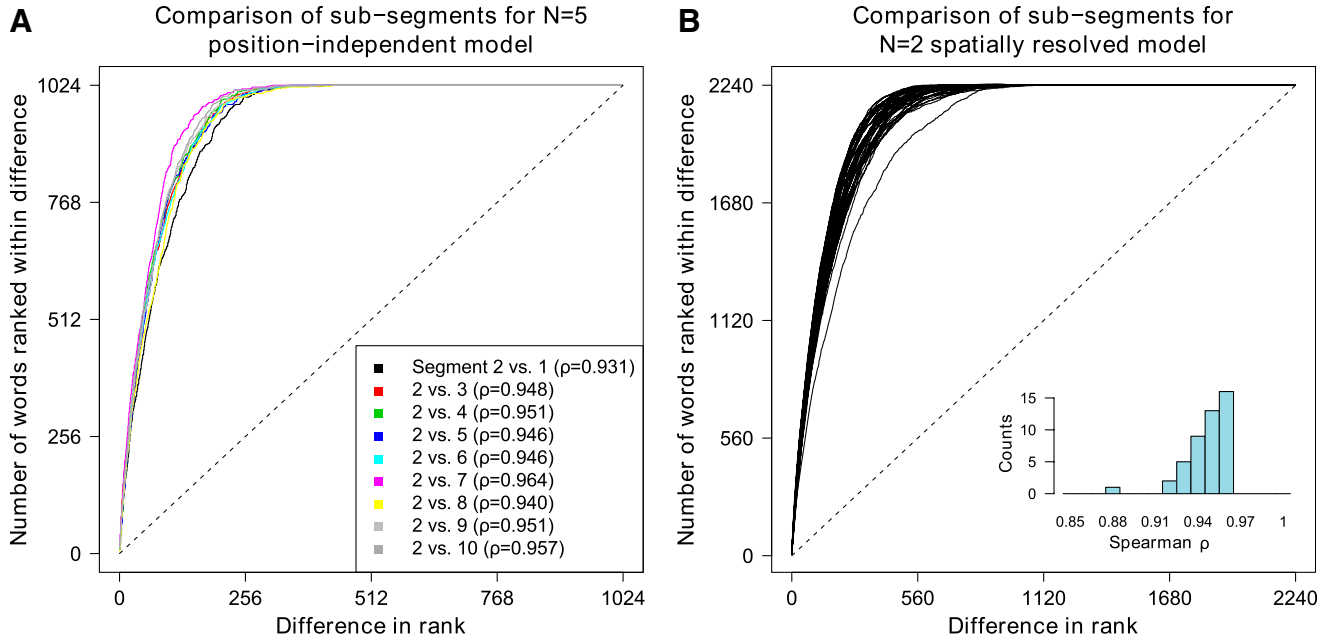

Fig. S11 Cross-validation of the $N = 5$ position-independent and $N = 2$ spatially resolved models in *S. cerevisiae*. (*A*) Rank-order plots of energies of 5 bp words: yeast genome is divided into four segments of equal size and the energy of each word is ranked using $N = 5$ position-independent models independently trained on each segment. Each curve shows the number of words whose ranks are separated by a given distance or less. Energies of 5 bp-long words contain contributions from all shorter motifs: $E(S) = \sum_{n=1}^{5} \sum_{\{\alpha_1 \ldots \alpha_n\}}^{4^n} n_{\alpha_1 \ldots \alpha_n} \epsilon_{\alpha_1 \ldots \alpha_n}$, where $n_{\alpha_1 \ldots \alpha_n}$ is the number of times a given word was found within the 5 bp-long sequence S and $\epsilon_{\alpha_1 \ldots \alpha_n}$ is the fitted energy of that word. (*B*) Rank-order plots of dinucleotide energies at each position predicted with $N = 2$ spatially resolved models independently trained on 47 segments of equal size. Dinucleotide energies at each position are computed using $E_{\alpha_i \alpha_{i+1}} = \epsilon_{\alpha_i \alpha_{i+1}} + \epsilon_{\alpha_i}$, $i = 4 \ldots 142$, and $E_{\alpha_{143} \alpha_{144}} = \epsilon_{\alpha_{143} \alpha_{144}} + \epsilon_{\alpha_{143}} + \epsilon_{\alpha_{144}}$ (*SI Text*) and ranked across all positions. The inset shows a histogram of rank-order correlation coefficients between dinucleotide energies trained on one of the segments, and all other segments.

Table S1 Correlation coefficients between nucleosome occupancy profiles

	Data				Model
	Zhang et al.1 in vitro	Kaplan et al.3 in vitro	Kaplan et al.3 in vivo, no CL	Kaplan et al.3 in vivo, CL	Zhang et al.1 in vitro, $N = 2$ PI
$N = 2$ PI models					
Zhang et al. 1 in vitro	0.60	0.75	0.58	0.41	1.00
Kaplan et al. 3 in vitro	0.59	0.76	0.58	0.40	0.99
Kaplan et al. 3 in vivo, no CL	0.57	0.74	0.56	0.38	0.98
Kaplan et al. 3 in vivo, CL	0.58	0.73	0.56	0.43	0.96
Zhang et al. 1 sonication	0.52	0.64	0.51	0.31	0.87
MNase	0.52	0.61	0.46	0.30	0.85
Zhang et al. 1 *E. coli*	0.55	0.68	0.52	0.42	0.90
Valouev et al. 4 *C. elegans*	0.46	0.59	0.45	0.39	0.72
Other models					
$N = 5$ PI	0.61	0.75	0.59	0.42	0.99
$N = 1$ PI	0.54	0.70	0.54	0.34	0.91
$N = 2$ three-region	0.62	0.75	0.58	0.41	0.99
$N = 2$ periodic	0.59	0.74	0.57	0.40	1.00
Spatially resolved	0.61	0.75	0.57	0.39	0.99
Kaplan et al. 2	0.60	0.79	0.59	0.40	0.89

PI—position-independent, CL—cross-linking. All models were trained on nucleosome maps from *S. cerevisiae* unless indicated otherwise. Models other than $N = 2$ position-independent models were fit to in vitro nucleosomes from Zhang et al. (1) Kaplan et al. (3) bioinformatics model was downloaded from http://genie.weizmann.ac.il/pubs/nucleosomes08/ and run on the yeast genome

Table S2 Table of rescaled dinucleotide energies

Species	*S. cerevisiae*		*E. Coli*		*C. Elegans*		MNase		Sonicated	
rank	word	energy	word	energy	word	energy	word	energy	word	energy
1	TT	1.76	TT	2.14	TT	1.57	TT	1.40	AT	1.30
2	AA	1.76	AA	2.14	AA	1.57	AA	1.40	TA	1.30
3	TA	1.10	TA	0.59	CG	1.36	AT	0.90	TT	1.07
4	AT	0.98	CT	0.26	GC	0.93	GA	0.62	AA	1.07
5	CT	0.27	AG	0.26	TA	0.71	TC	0.62	CT	0.31
6	AG	0.27	AT	0.25	CC	0.40	AG	0.32	AG	0.31
7	TC	0.19	GG	0.09	GG	0.40	CT	0.32	GA	0.16
8	GA	0.19	CC	0.09	AT	0.06	TA	0.32	TC	0.16
9	AC	-0.50	GC	-0.15	AG	-0.69	TG	0.04	TG	0.05
10	GT	-0.50	GA	-0.36	CT	-0.69	CA	0.04	CA	0.05
11	CA	-0.55	TC	-0.36	GT	-0.73	GT	-0.24	AC	-0.09
12	TG	-0.55	TG	-0.84	AC	-0.73	AC	-0.24	GT	-0.09
13	GG	-0.81	CA	-0.84	GA	-0.80	CC	-0.77	GG	-0.86
14	CC	-0.81	CG	-1.04	TC	-0.80	GG	-0.77	CC	-0.86
15	GC	-1.40	AC	-1.12	TG	-1.28	CG	-1.97	GC	-1.79
16	CG	-1.42	GT	-1.12	CA	-1.28	GC	-1.99	CG	-2.09

Table of dinucleotide energies predicted by training $N = 2$ position-independent models on several nucleosome positioning maps and nucleosome-free control experiments. Energies for each model have been rescaled to the variance of 1 a.u.